Review

New progress in development of ferroelectric and piezoelectric nanoceramics

Xiao-Hui WANG[a],[*], I-Wei CHEN[b], Xiang-Yun DENG[a], Yu-Di WANG[b], Long-Tu LI[a]

[a]*State Key Laboratory of New Ceramics and Fine Processing, School of Materials Science and Engineering, Tsinghua University, Beijing 100084, China*
[b]*Department of Materials Science and Engineering, University of Pennsylvania, Philadelphia, PA 19104-6272, USA*

Abstract: There has been great progress in the last decade in the synthesis of nanopowders with highly controlled size and size distribution. Meanwhile, the development of an unconventional pressureless two-step sintering strategy enabling densification without grain growth provides a novel technology suitable for commercial production of nanograin ceramics. The particular interest concerning bulk dense nanograin ceramics is the manifestation of ferroelectricity, which remains a fundamental issue to be understood and exploited. Combining the best powder synthesis and optimized two-step sintering, high-density barium titanate (BT) and related nanograin ceramics have been fabricated to allow for a detailed determination of the size effect on nanometer-scale ferroelectricity and piezoelectricity of fundamental and industrial interest. These include dense ceramics of undoped BT with an average grain size down to 5 nm, and of $(1-x)BiScO_3-xPbTiO_3$ (BSPT) solid solutions with an average grain size down to 10 nm. Here we review the fabrication methods of high-density BT and BSPT nanoceramics and the major findings of the size effect on their microstructure, phase transition and electrical properties. Robust ferroelectricity is demonstrated for the first time in 5 nm BT nanoceramics, while strong local piezoelectricity is present in 10 nm BSPT nanoceramics.

Keywords: nanoceramic; ferroelectric; piezoelectric; barium titanate; size effect

1 Introduction

Barium titanate (BaTiO$_3$, BT) of the perovskite ABO$_3$ type has played an important part in the modern ceramic industry because of its advantageous ferroelectric, piezoelectric and dielectric properties, finding applications in multilayer ceramic capacitors, printed circuit boards, random access memory, positive temperature coefficient of resistance thermistors,

piezoelectric sensors, and actuators [1–4]. Since the 1970s, polycrystalline multilayer ceramic capacitors (MLCCs) made of ferroelectric BT have been deployed for ever-expanding applications, aided in recent years by incorporating nickel (Ni, a so-called base metal) electrode made feasible by low temperature firing. Driven by the demand of ever smaller sizes, higher performance and lower component costs in electronic industry, the evolution of MLCCs with base metal inter-electrodes (BME) and thinner dielectric layers is continuing [5–7]. MLCCs capable of 10^{-13} F to 10^{-4} F are used in products from

---

* Corresponding author.
E-mail: wxh@mail.tsinghua.edu.cn

computers to automobiles. Currently, 10^{13} new pieces of MLCCs enter the market every year. As their layer thickness decreases below 1 μm and the attendant ceramic grain size (GS) shrinks below 100 nm, MLCC represents the most significant nanograin ceramics in use today. This prospect is expected to continue in the next decade.

The driving force toward nanograin MLCC ceramics has come from not only component miniaturization but also performance. However, it is well known that once the grain size is decreased below 1 μm, a rapid decrease of dielectric constant (K) is common. This drop may pose a limitation to the miniaturization of MLCCs since miniaturization of MLCCs usually goes hand in hand with grain size reduction. Typically, the dielectric layer has to comprise of at least 5–7 grains across the thickness, for reasons of layer flatness, high reliability and uniform properties. It follows that in a layer of 0.5–0.7 μm thick, the grain size must be maintained below 100 nm. Consequently, it is of great practical interest to prepare dense nanograin BT and other related ceramics and to investigate their dielectric, ferroelectric and piezoelectric characteristics: the findings should provide important directions for the design of next generation MLCCs.

Grain size has a profound influence on the crystal structure and properties of BT ceramics [8−10]. Coarse-grain BT ceramics undergo several phase transitions as a function of temperature. Starting from a low temperature at about −75 ℃, BT begins to transform, from a rhombohedral (R) to an orthorhombic (O) structure, then to a tetragonal (T) phase at about 5 ℃, and finally to a cubic (C) phase at around 130 ℃ [11]. The C→T phase transition is a ferroelectric transition; therefore, it also drives the formation of polydomain subgrains or domains, which minimize electrostatic and elastic energies in the polar, non-isometric state. It has been generally speculated that there is a critical grain size below which ferroelectricity—embodied by the ferroelectric T to C distortion—is lost. Structural studies on BT ceramics by Frey and Payne [9], however, indicated the retention of a long-range cooperative driving force for the distortion at a grain size well below 100 nm. Other estimates have placed the critical size in the range of 10–30 nm for BT ceramics [12]. On the other hand, recent studies [12−14] on dielectric properties have shown that there is a "dilution effect", caused by the presence of a lower permittivity (nonferroelectric)

dead layer along the grain boundary, which can considerably lower the permittivity in submicron and nanocrystalline BT ceramics and thin films. The dead layer is not necessarily a second phase; it could be accounted by a crystalline BT layer with a more disordered/defective structure or a ferroelectric layer that is non-switchable because of polarization clamping by surface or grain boundary. The latter could be due to mechanical origin or electrical origin: in this scenario, ferroelectric perovskite has a correlation length of about 1–3 nm, which is the scale within which the polarization is clamped by the dielectric boundary, thus providing an estimate of the dead layer thickness. Whether this picture is entirely correct or not is currently not known. Experimentally, though, Buscaglia *et al.* [15] already reported a dense (spark plasma sintered) 30 nm (GS) BT ceramic which has a high dielectric constant but a frozen macroscopic polarization suggesting a strong clamping but little dilution effect.

Obviously, whether nanograin BT can provide an elevated K itself is an important practical issue which has been repeatedly questioned in the literature. In the coarse-grain regime, K has a well-known maximum at GS ≈ 1 μm [9], below which K decreases. In our 2006 work on a dense BT ceramic fabricated by two-step sintering method, we found microscopy evidence of ferroelectric polydomain state in samples with an average grain size as small as 8 nm [16]. We also found it to display a robust K–temperature (T) performance, with a very low dielectric loss and a clear evidence of multiple dielectric/ferroelectric transitions. This implies that a ceramic capacitor with a layer thickness of 40–50 nm (containing 5–7 grains of 8 nm sized) is still viable. To predict the critical grain size, a phenomenological thermodynamic theory with an additional consideration of stress effects caused by surface bond contraction was proposed by Sun *et al.* [17]. It predicts changing trends in phase transitions and the critical grain size for the disappearance of the ferroelectric phases, including two opposite relationships between the grain size and (two kinds of) stresses. The size that leads to the disappearance of ferroelectric phases at room temperature is found at about 5.2 nm. When the grain is less than 2.5 nm, the ferroelectric phases are fully absent over the entire temperature region. Most recently, to determine whether it is feasible to fabricate sub-5 nm ceramics, we fabricated ultrafine BT nanocrystalline powders of 3–5 nm using a one-step solvothermal method [18],

and then obtained, by two-step sintering, dense BT ceramics with a grain size of 5 nm, which set the record for the finest dense bulk nanograin material. This is reassuring for the MLCC industry and augurs well for the status-quo MLCC fabrication method (with tape-casting of green layers, screen printing of electrodes and co-firing of $BaTiO_3$/electrode stacks of hundreds of layers): with incremental changes and advances, they may continue for the foreseeable future.

On the piezoelectric side, $(1-x)BiScO_3-xPbTiO_3$ (BSPT) is a solid solution which was first investigated by Eitel *et al.* [19] in 2001 as a member of a new family of high-temperature piezoelectric ceramics. They investigated a series of complex perovskites with the general formula $Bi(Me^{3+})O_3-PbTiO_3$ ($Me^{3+} = Sc^{3+}$, Fe^{3+}, In^{3+}, Yb^{3+}, etc.) that have a large deviation from unity for the tolerance factor t of Goldschmidt [20]. Among these solid solutions, BSPT is the only one that has a tolerance factor ($t = 0.907$) less than that of $Pb(Zr,Ti)O_3$ (PZT, $t = 0.96$) and still maintains a stable perovskite structure under atmospheric conditions. It exhibits a high T_C of 450 ℃ at compositions near the morphotropic phase boundary (MPB) and has outstanding piezoelectric properties (electromechanical coupling factor $K_p = 0.57$, piezoelectric constant $d_{33} = 450$ pC/N). Extensive studies have since been carried out on BSPT ceramics [19,21–31], single crystals [32–36] and thin films [37–43], confirming their high Curie temperature, excellent ferroelectric/piezoelectric properties and robust thermal stability. For example, in our previous study on BSPT ceramics [25], we obtained the best piezoelectric properties at $x = 0.635$ (near the MPB): $d_{33} = 700$ pC/N and $K_p = 0.632$, with a Curie temperature of 446 ℃, all higher than those of PZT. Because of these excellent properties, BSPT is a promising candidate material for high-temperature sensors and actuators. On the other hand, investigations of the grain size effect on piezoelectric ceramics [44] are still few and there is no consistent conclusion on this subject for nanograin BSPT ceramics. Using two-step sintering, we have fabricated dense BSPT ceramics with average grain size from 1 μm down to about 10 nm. These ceramics thus provide an opportunity for studying the grain size effect on BSPT ceramics.
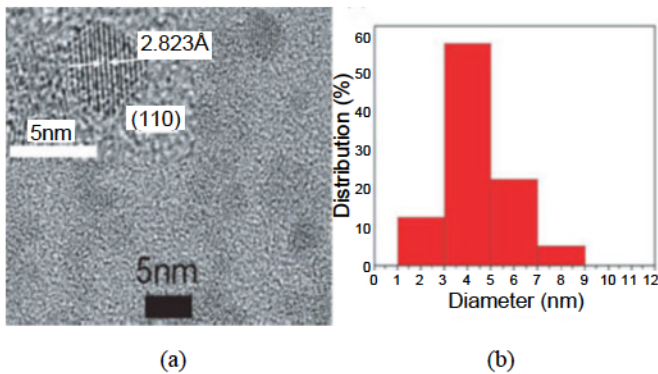
In the following, we will provide an overview of the methods for fabricating dense BT and BSPT nanograin ceramics and the investigation of the grain size effect on their microstructures, phase transition and dielectric, piezoelectric and ferroelectric properties. The existence of the ferroelectric phase in these ceramics at room temperature will be probed by the hysteresis loops of polarization reversal, as is the corresponding local ferroelectric switching hysteresis being recorded by piezoresponse force microscopy. These results provide the first experimental evidence for ferroelectricity and piezoelectricity in bulk dense below-10 nm BT and BSPT ceramics with their respective high Curie temperatures.

2 Preparation of nanograin ceramics by two-step sintering

2.1 BaTiO₃

Nanopowders of BT with well-defined crystallinity, high purity and a narrow particle size distribution are generally required for manufacturing nanograin ceramics. Low crystallinity is itself a problem emanating from the size effect, but hydroxyl ion incorporation from the air is another reason for low crystallinity. The development of new methods to synthesize monodispersed BT nanocrystals will facilitate the studies of the size effect. Hydrothermal synthesis of ceramic powders with well-controlled parameters (concentration, pH and temperature) has been widely reported, especially for low-temperature preparation of relatively single-phase products [45,46]. This method has been used to prepare highly dispersed BT powders with a particle size smaller than several tens of nanometers. However, aqueous hydrothermal systems mostly produce cubic BT phase powders; to obtain the tetragonal phase capable of ferroelectricity annealing at high temperature is necessary, but with it crystallite size growth and powder aggregation are inevitable. Thus, non-aqueous reaction approaches may have considerable advantages in controlling crystallization and particle growth. Monodispersed BT nanocrystals with the tetragonal structure have been synthesized using a one-step solvothermal method in our laboratory [18]. They have an average size of about 3–5 nm with a narrow distribution, with a high-resolution transmission electron microscopy (HRTEM) image illustrated in the inset of Fig. 1(a), which indicates well-crystallized nanoparticles. A lattice tetragonality (c/a ratio) of 1.0069 can also be discerned from the TEM micrograph in Fig. 1(a) for 5 nm particles. The particle size distribution with an

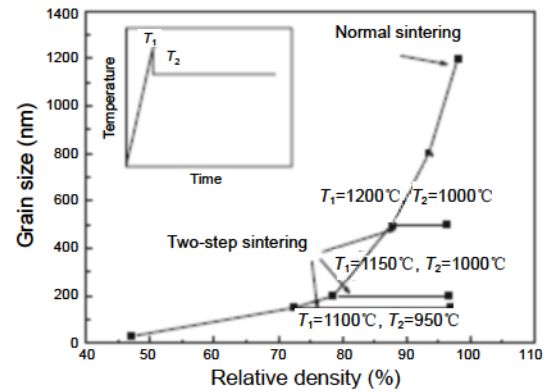(a)   (b)

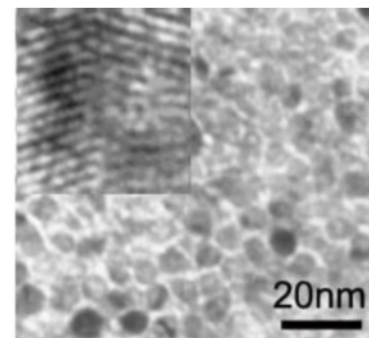**Fig. 1**   (a) TEM image and (b) size distribution of 5 nm BT nanoparticles.

average size of 5 nm is shown in Fig. 1(b).

Two-step sintering (TSS) was invented to allow fabricating dense nanograin ceramics Y_2O_3 (a highly refractory oxide with a melting point of 2600 ℃) without pressure [47]. It has since been proved to be a highly efficient method to prepare other kinds of dense nanograin bulk ceramics, including both oxides and nonoxides [48−53]. In this method, the ceramic is first fired at a higher temperature T_1 to reach a critical density (typically 75% so that the average pore is relatively small compared to the grains, thus acquiring capillary driving force to spontaneously sinter and not to coarsen). Subsequently, the temperature is lowered to T_2 to allow further densification all the way to full density. The remarkable feature of this procedure is that there is no grain growth during the second step densification apparently because the four-grain junctions are "frozen" thus resisting grain boundary migration even though grain boundary diffusion still proceeds. This is rather unique and completely unlike the case in normal sintering in which final stage densification is always accompanied by rapid grain growth. This method was initially applied to Y_2O_3, which we sintered to full density at 1000 ℃ without doping, or at 800 ℃ with 1 cation% Mg doping [47,54]. It was also successfully used to sinter undoped BT ceramics (fully dense at as low as 750 ℃) [51]. The dramatic contrast of the microstructure development of BT ceramics in normal sintering and in TSS can be seen in Fig. 2, where several grain size–density trajectories are depicted. It is clear that grain growth during the second-step sintering ($T_2 < T_1$) was completely suppressed.
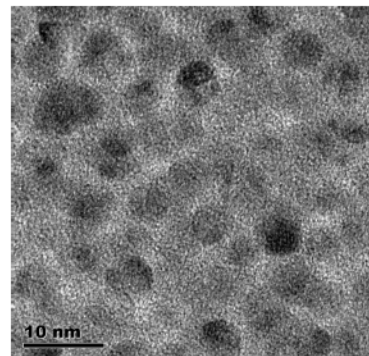
Dense (99.6% of theoretical density) BT ceramics around 8 nm were also obtained by us using TSS [16,55]. Figure 3(a) shows its microstructure under TEM. The grain size is very uniform with a narrow distribution. The inset of Fig. 3(a) is a high-resolution
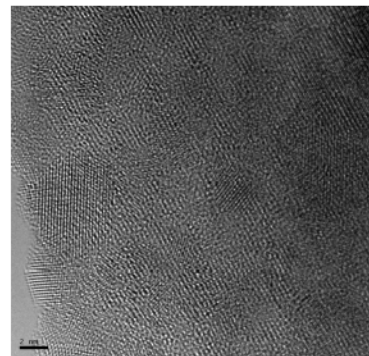

Fig. 2   Grain size versus density for BT ceramics sintered by two-step sintering and by normal sintering.

(a) 8 nm TEM (inset HRTEM)

(b) 5 nm TEM

(c) 5 nm AC-HRTEM

Fig. 3   TEM and HRTEM images of BT ceramics with grain sizes of 8 nm and 5 nm.

image of the 8 nm sample, which is free of impurity phase and the grain boundary is about 0.4 nm thick. This grain boundary thickness is roughly equal to the lattice constant of BT and is much smaller than the data for BT nanoceramics in the literature. Recently, using 3–5 nm nanopowders of BT (by solvothermal synthesis) mentioned above, aided by cold isotropic pressing (CIP) with an ultrahigh pressure (6 GPa), we obtained dense BT nanoceramic with a grain size of 5 nm again by TSS (Figs. 3(b) and 3(c), the latter is an aberration-corrected HRTEM (AC-HRTEM) image) [56], which is the finest BT ceramic ever obtained.

Employing the two-step sintering strategy without applying a high pressure during CIP, a series of high-density bulk BT ceramic samples with grain size ranging from micrometer to 30 nm scale have also been prepared [56−58]. Table 1 lists some of the successful two-step sintering experiments (BaTiO$_3$-1– BaTiO$_3$-18) using 10 nm, 30 nm and 100 nm BT powders. These experiments all achieved high density ($\geqslant$ 96%) without grain growth in the second step. Larger grained samples were also obtained by increasing T_2 to allow some grain growth (BaTiO$_3$-19: GS = 4.32 μm and BaTiO$_3$-20: GS = 8.61 μm, in Table 1). Together, these ceramics provided a set of samples for the systematic investigation of the size effect on tetragonal distortion, phase transition, Curie temperature and dielectric properties to be described later.

2. 2   (1−x)BiScO₃−xPbTiO₃

A citrate sol–gel method was utilized to synthesize BSPT nanopowders with a near MPB composition (x =

0.635−0.64) and grain size of 6−10 nm [24,25]. Optimum parameters of two-step sintering were investigated using the data summarized in Table 2 and Fig. 4 [24]. The wedge shape region of the T_2 window for successful sintering in Fig. 4 resembles that for Y_2O_3 and $BaTiO_3$ (see our previous publications [47,51]), suggesting similar thermodynamics and kinetics underlying two-step sintering in different ceramics. Using these conditions, highly dense MPB BSPT ceramics with homogeneous fine grains as small as 200 nm can be obtained at 800 ℃ without sintering aid [24,25].

Ceramics of much finer grain size can also be obtained from nanopowders by introducing additional
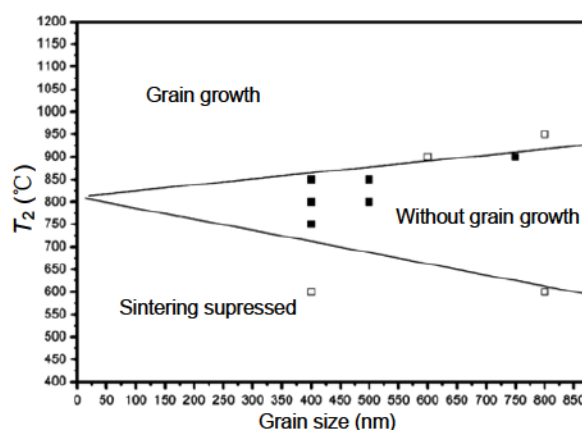

Fig. 4   Kinetic window for reaching full density without grain growth for BSPT ceramics. Solid symbols present successful sintering conditions, and open symbols indicate those that cannot reach high density (below the lower boundary) or cause uncontrolled grain growth (above the upper boundary).

Table 1   Two-step sintering results of BT ceramics (initial powder sizes of 10 nm, 30 nm and 100 nm)

Sample	ρ_0 (%)	After 1st-step sintering				After 2nd-step sintering			
		T_1 (℃)	t_1 (h)	ρ_1 (%)	GS$_1$ (nm)	T_2 (℃)	t_2 (h)	ρ_2 (%)	GS$_2$ (nm)
BaTiO$_3$-1[*]	61	950	0	86	33	900	2	98.0	35
BaTiO$_3$-2[*]	46	980	0	78	68	900	4	97.0	70
BaTiO$_3$-3[**]	46	1100	0	73	148	900	20	96.2	150
BaTiO$_3$-4[**]	46	1100	0	73	148	950	20	97.1	150
BaTiO$_3$-5[**]	46	1150	0	78	200	900	20	96.3	200
BaTiO$_3$-6[**]	46	1150	0	78	200	1000	20	97.2	200
BaTiO$_3$-7[**]	46	1180	0	83	296	950	20	97.0	300
BaTiO$_3$-8[**]	46	1180	0	83	296	1000	20	97.2	300
BaTiO$_3$-9[**]	46	1200	0	87	495	850	20	96.0	500
BaTiO$_3$-10[**]	46	1200	0	87	595	900	20	96.3	500
BaTiO$_3$-11[**]	46	1200	0	87	495	1000	10	97.2	500
BaTiO$_3$-12[**]	46	1200	0	87	495	1100	10	97.0	500
BaTiO$_3$-13[**]	46	1230	0	90	795	850	20	97.5	800
BaTiO$_3$-14[**]	46	1230	0	90	795	1000	20	98.0	800
BaTiO$_3$-15[***]	48	1310	0	88	990	800	24	96.4	990
BaTiO$_3$-16[***]	48	1310	0	88	990	850	24	96.4	1020
BaTiO$_3$-17[***]	48	1340	0	90	1950	900	24	98.0	1970
BaTiO$_3$-18[***]	48	1340	0	90	1950	950	24	97.4	2210
BaTiO$_3$-19[***]	48	1340	0	90	1950	1050	24	96.8	4320
BaTiO$_3$-20[***]	48	1340	0	90	1950	1100	24	96.5	8610

[*]Initial powder size of 10 nm; [**] initial powder size of 30 nm; [***] initial powder size of 100 nm.

Table 2   **Parameters of two-step sintering for BSPT ceramics**

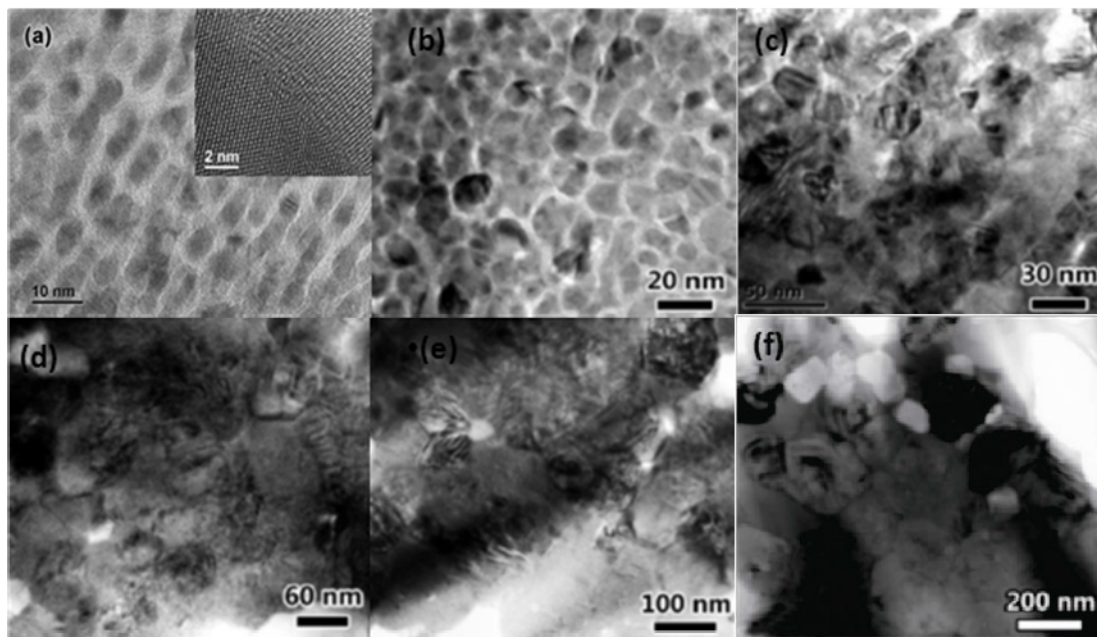| Sample	Sintering method		*t* (h)	Relative density (%)	GS (nm)
	T_1 (℃)	T_2 (℃)			
A	930	800	8	71.8	350
B	960		8	89.0	390
C_1		750	8	96.1	400
C_2	1000	800	8	98.8	400
C_3		850	8	95.8	400
C_4		900	8	98.0	600
D	1020	800	8	97.9	470
E_1		800	8	98.1	497
E_2	1050	850	8	98.5	497
E_3		900	8	97.4	750
E_4		950	8	95.5	795

practice of high-pressure consolidation during forming or spark plasma sintering (SPS). Due to their extremely large specific surface area, BSPT nanopowders are rather sensitive to sintering temperature and holding time, and volatile additives such as Pb and Bi cannot be used since they tend to cause rapid grain growth. BSPT ceramics of 80 nm grain size were already obtained by Alguero *et al.* [59] using SPS, and by SPS Amorín *et al.* [60] further reduced the average grain size to 28 nm. However, possibly due to the activation of particle surface and the high ion mobility during the SPS process, the grain size of BSPT ceramics is apparently very sensitive to the sintering temperature and mechanical pressure, thus difficult to control. Combining SPS and two-step sintering methods, we obtained BSPT samples with an average grain size ranging from 23 nm to 70 nm [61]. Moreover, adopting

a practice previously used for preparing 5–8 nm BT ceramics [55,56], we held BSPT nanopowders at ~5.5 GPa for 15 min at room temperature to enable plastic deformation, which allows a green body with a relative density of about 83% to form [62], then used two-step sintering (conditions in Table 3) to obtain ceramics with a grain size as small as 11 nm. This is the finest BSPT ceramics ever reported.

TEM micrographs of these BSPT nanoceramics are shown in Fig. 5. The grain size of sample S_1 (6–10 nm) lies in the same range of particle size of the starting nanopowders. The influence of T_1 is clearly important by comparing samples S_1 and S_4, which used the same T_2 and very similar holding time but different T_1, resulting in a three-fold grain size difference. However, a long holding time at the same T_2 can also cause grain growth, as evident from comparing samples S_5 and S_6, which used identical T_1 and T_2 but different holding time. In general, with the increase of the sintering temperature, the grain size distribution becomes wider.

Table 3   **Two-step sintering schedules using BSPT green body of 83% relative density**

Sample	T_1 (℃)	T_2 (℃)	*t* (h)	ρ_2 (%)	GS (nm)
S_1	850	700	31	95.6	11
S_2	900	700	24	96.6	21
S_3	900	750	24	96.4	25
S_4	950	700	24	95.7	33
S_5	900	800	12	96.8	60
S_6	900	800	24	95.9	80
S_7	950	800	12	97.7	114

Fig. 5   TEM images of BSPT nanoceramics with grain sizes of (a) 11 nm (inset AC-HRTEM), (b) 21 nm, (c) 33 nm, (d) 60 nm, (e) 80 nm and (f) 114 nm.

Note that although samples S_1 and S_2 seem to have thick grain boundaries in Figs. 5(a) and 5(b), this is an imaging artifact since HRTEM imaging shown in the inset of Fig. 5(a) clearly reveals a dense and sharp grain boundary region. Such artifact is usually unimportant for imaging grains above 30 nm, as in sample S_3, Fig. 5(c), in which the grain boundary region seems quite thin and comparable with the morphology usually observed in BSPT ceramics with micrometer-sized grains.

3 Microstructures and properties of nano BaTiO$_3$ ceramics

3.1 Microstructures and structural transitions

3.1.1 Raman spectra

Raman spectroscopy can provide a very sensitive measurement of the local crystal symmetry in powders, polycrystals and single crystals, such as PbTiO$_3$ and BaTiO$_3$ [63−65]. In the following, we describe our observations of Raman spectroscopy of BT powders and nanoceramics obtained using a confocal microscopic Raman spectrometer (RM2000, Renishaw, UK). To provide a reference, Raman spectra of a ceramic sample with GS = 3 μm were first collected. As shown in Fig. 6(a), in the temperature range of −190–500 ℃, such spectra feature distinct C/T/O/R dielectric transitions.

Concerning the above spectra, while symmetry-characteristic spectra (e.g., 200 ℃ for the C phase, 100 ℃ for the T phase, 0 ℃ for the O phase and −150 ℃ for the R phase) might be designated, the sensitivity of BT Raman spectra to both optical and microstructural details (e.g., polarization, mode–mode interference, orientation, single-domain vs. multi-domain vs. polycrystal) demands a more cautious interpretation. It is known that the 310 cm^{-1} (sharp) and 715 cm^{-1} bands are forbidden in the C symmetry, the peak position of the 240–270 cm^{-1} broad band discontinuously drops during the T/O transition, and the sharp multi-peak at 170–190 cm^{-1} band is an R characteristic, although in both O and T symmetries it still manifests as a weak, diffuse feature. Judging from the gradual nature of changes in the Raman spectra, this may also apply to other transitions suggesting the coexistence of different symmetries over a broad range of temperatures at least at the local structure level. Such ambiguity defying the use of simple

symmetry-dictated selection rules is not unique to BaTiO$_3$; a more extreme case is nominally cubic ZrO$_2$ (stabilized by cations causing oxygen vacancies), which is well-known to have Raman bands that are forbidden in the cubic fluorite structure [66]. (This is possible because cubic ZrO$_2$ actually has a non-fluorite-like seven-fold-coordinated local structure, as clearly revealed by extended X-ray absorption fine structure (EXAFS) spectroscopy [67–69], but these seven-fold-coordinated units are so arranged as to yield a set of cubic-fluorite-like diffraction planes that are sufficiently flat when viewed on the longer length scale by the diffracting radiation. This interpretation is perhaps also appropriate for lower-symmetry phases of BaTiO$_3$.)

The above information allowed us to definitely identify, in the BT ceramic sample of GS = 50 nm (Fig. 6(b)), R symmetry at −190−−150 ℃ (double-peak at 170–190 cm^{-1}) and T/O transition at 50–100 ℃ (discontinuous shift of 240–270 cm^{-1}), which are sufficient to establish the existence of all three (T/O/R) symmetries. Note that the nominally "C" spectrum at 200 ℃ still has weak features at 310 cm^{-1} and 715 cm^{-1} indicating T remnants. Therefore, the C/T transition is rather diffuse in the polycrystal. Figures 6(c) and 6(d) show the Raman spectra of two other dense BT ceramics, with GS = 8 nm and 5 nm, respectively; the spectra of 5 nm nanopowders are also shown in Fig. 6(e). All featured peaks and their temperature evolutions seen in the Raman spectra of coarse-grain ceramics mentioned above are seen in these spectra. Furthermore, the nominally "C" spectrum at 290 ℃ still has weak features at 310 cm^{-1} and 715 cm^{-1}, indicating that the T remnants can survive above the Curie temperature, 290 ℃. This suggests that all polar phases in coarse-grain ceramics still exist in nanoceramics and nanopowders, at least down to a size of 5 nm, and that they should all undergo R→O→T→C phase transitions as the temperature rises [70,71]. In particular, the spectroscopy behavior of 5 nm powders and 5 nm dense ceramics is similar, as is the behavior of an 8 nm BT ceramic reported in our previous study [16].

3.1.2 High-resolution synchrotron X-ray diffraction

Quantitative phase analysis of nanograin BT ceramics is hampered by the size broadening of diffraction peaks when using conventional diffraction techniques. Therefore, we performed high-resolution synchrotron X-ray diffraction to study the phase evolution and
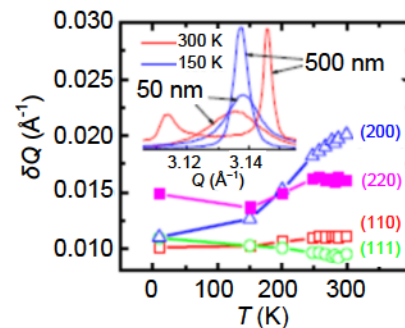
Fig. 6 Raman spectra of BaTiO$_3$: (a) 3 μm ceramic used as reference, (b) 50 nm ceramic, (c) 8 nm ceramic, (d) 5 nm ceramic and (e) 5 nm powders. All are shown as a function of temperature from −190 ℃ to 500 ℃.

coexistence of these ceramics (5–100 nm and 150–450 K) [72]. Our results indicate that, as temperature rises, nanograin BT still follows the same phase sequence, but the phase boundaries become more diffusive and more than one phase may coexist between 200 K and 450 K. The diffraction patterns were collected at APS 11-BMB, Argonne National Laboratory, with a resolution $<2\times10^{-4}$ $\Delta Q/Q$. The temperature was controlled within ±1 K. All the diffraction data were analyzed through Rietveld refinement using the General Structure Analysis System (GSAS) software package [73], including the lattice parameters, atomic positions, thermal parameters and the fractions of R, O, T and C phases.

For the BT ceramic of GS = 50 nm, although there is no peak splitting in the diffraction patterns (inset in Fig. 7), the non-monotonic temperature dependence of the diffraction peak width δQ reveals underlying phase transitions (errors in Fig. 7 are much smaller than the size of the symbols and the width of the diffraction curves). Specifically, since peak splitting in single crystal is most pronounced at the (200) reflection in the

(high-temperature) T phase but most pronounced at the (220) reflection in the (low-temperature) R phase [74], it is unlikely to be a mere coincidence that the same trend is observed in Fig. 7 in the temperature variation of δQ of the "unsplit" (200) reflections and (220) reflections. If instead we take δQ as being caused by the combined effect of peak splitting and phase mixing, we can analyze the δQ data to obtain the phase fractions; this is shown as a function of temperature in Fig. 8. Quite similar results were also obtained for a

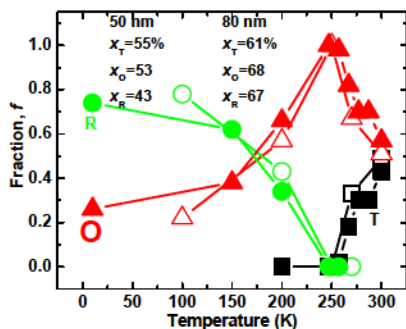**Fig. 7** Synchrotron X-ray structure analysis of nanograin BaTiO$_3$ ceramic (GS = 50 nm).

Fig. 8 Phase analysis of nanograin BaTiO$_3$ ceramics (GS = 50 nm and 80 nm).

ceramic of GS = 80 nm.

A parallel study of BT nanopowders was also performed using the same diffraction method. Table 4 gives the phase fractions of BT nanopowders with particle size 5–100 nm at various temperatures. Except for the R phase at 150 K, all other diffraction patterns must be fit with two or three phases, R+O, R+O+T, O+T and O+T+C, in the sequence of increasing temperature. Compared to coarse-grain ceramics and coarse powders, the temperature range of R, O, T and C phases are all extended, resulting in phase coexistence over a wide temperature range. This trend is consistent with the observation in nanograin ceramics. In particular, with decreasing particle size or grain size, the temperature of the C to T transition decreases, while the temperatures of the R to O and O to T transitions increase. Meanwhile, although the phase boundaries become diffuse in Fig. 9, even the smallest sized BT powders are still ferroelectric over a wide temperature range, making them potentially suitable for practical, ferroelectricity-related applications.

Nano BT powders and ceramics with very small sizes and very large surface areas are likely to have a large number of defects on the surface and grain boundaries, which may give rise to compressive stresses. These internal stresses may alter relative phase stability in a complicated manner [18,75], causing shift of phase boundary, diffuse transition and phase coexistence. (Long-range shear stresses have also been speculated in the literature, although they are unlikely since they can be easily relaxed by grain boundary dislocations and related defect constructs.) In addition, there seems to be some evidence that the evolution may not be monotonic, with possible phase reentrance as shown in Fig. 10 for 20 nm BT powders, suggesting that very small BT powders may sustain ferroelectricity after all. Further experimental studies (which may be challenging) to place these theoretical hypotheses and initial observations on a firmer footing are needed to reach a better understanding of ferroelectricity in a nanograin/nanopowder setting.
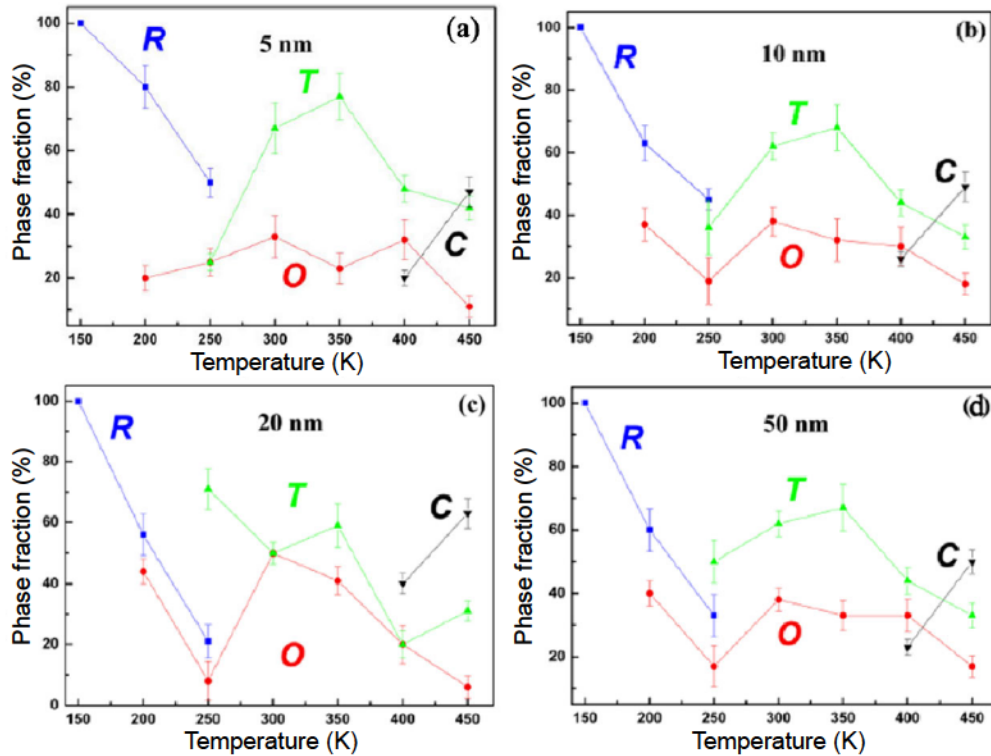
3. 2 Size effect on ceramic properties

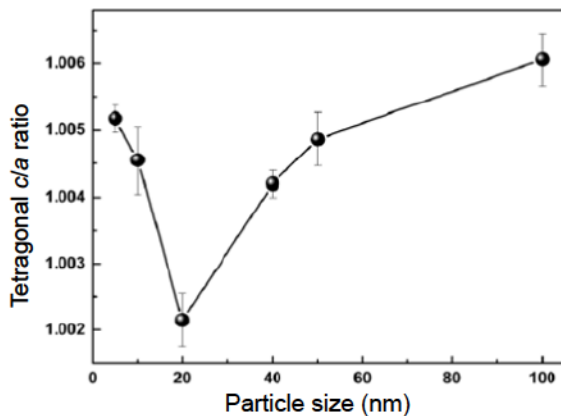### 3. 2. 1 Dielectric and ferroelectric properties

In the coarse-grain regime, relative dielectric constant K has a well-known maximum at GS $\approx$ 1 µm [9], below which K decreases since there is no domain wall movement. Whether nanograin BT can provide an elevated K has been repeatedly questioned in the literature, but no reliable data over a large range of grain size exist in the past. Using high-purity two-step sintered ceramic samples with grain size from nanometer to micrometer, we have investigated this subject. To remove the influence of moisture, which is especially pronounced at small grain size, dielectric measurements reported below were all performed in vacuum after the samples were first baked *in situ*.

Table 4 Phase fractions of nano BaTiO$_3$ powders as functions of particle size and temperature (unit: %)

Particle size	Tempertature						
	150 K	200 K	250 K	300 K	350 K	400 K	450 K
100 nm	R (100)	R+O (64+36)	R+O+T (25+25+50)	O+T (25+75)	O+T (20+80)	O+T+C (32+54+14)	O+T+C (28+24+48)
50 nm	R (100)	R+O (60+40)	R+O+T (33+17+50)	O+T (38+62)	O+T (33+67)	O+T+C (33+44+23)	O+T+C (17+33+50)
40 nm	R (100)	R+O (58+42)	R+O+T (22+13+65)	O+T (47+53)	O+T (38+62)	O+T+C (21+44+35)	O+T+C (15+33+52)
20 nm	R (100)	R+O (56+44)	R+O+T (21+8+71)	O+T (50+50)	O+T (41+59)	O+T+C (20+40+40)	O+T+C (6+31+63)
10 nm	R (100)	R+O (63+37)	R+O+T (45+19+36)	O+T (38+62)	O+T (32+68)	O+T+C (30+44+26)	O+T+C (18+33+49)
5 nm	R (100)	R+O (80+20)	R+O+T (50+25+25)	O+T (33+67)	O+T (23+77)	O+T+C (32+48+20)	O+T+C (11+42+47)

Fig. 9 Phase fraction evolutions of BaTiO$_3$ powders as a function of temperature with particles sizes of (a) 5 nm, (b) 10 nm, (c) 20 nm and (d) 50 nm.

Fig. 10 *c/a* ratio of tetragonal phase BaTiO$_3$ powders as a function of particle size at room temperature.

As shown in Fig. 11, all the temperature spectra of K show a discernible C to T phase transition. In comparison, the low-temperature transitions are much weaker and broader. At smaller grain size, they appear as diffuse humps on a positively sloping background that in part is the low-temperature tail of the C/T transition. We identify the transition temperatures at the minimal $\mathrm{d}^2K/\mathrm{d}T^2$, since this procedure largely removes the distortion caused by the sloping background (its $\mathrm{d}^2K/\mathrm{d}T^2 \approx 0$). As shown in Fig. 12, over the grain size range of 50–800 nm, the transition temperatures determined show a steady decrease with grain size of about 12 ℃ for the C/T transition, in contrast to a steady increase of a similar amount for the T/O transition and about 20 ℃ for the O/R transition. The temperature for the C/T transition of the 50 nm sample (115 ℃) agrees with that reported for an SPS BT of nominally the same grain size [76]. Meanwhile, although the T/O/R transitions have not been reported before for GS < 300 nm, the trend of increasing transition temperature with smaller grain size is the same as seen in coarse-grain BT (1.1–53 μm) [77]. Moreover, identical temperature spectra of relative dielectric constant with C/T/O/R transitions in cooling and heating were observed (not shown), indicating the behavior is rather robust. Therefore, although for smaller grain size (down to 50 nm) all transitions are very broad indeed, nanograin ceramics still have structural distortions following similar trends as those of coarse-grain ceramics.
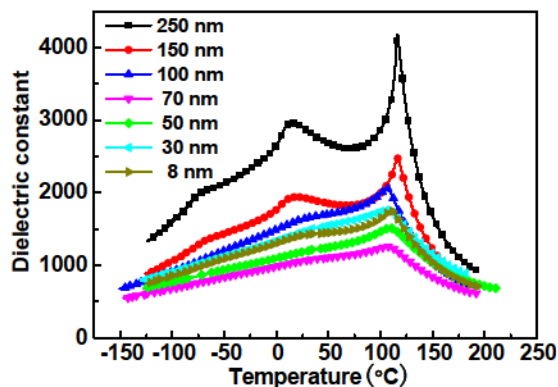
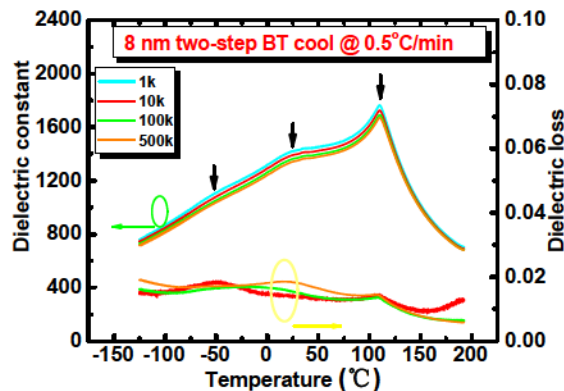**Fig. 11** Temperature spectra of dielectric constant for BT ceramics during cooling.

Fig. 12 Temperatures of C/T, T/O and O/R transitions versus grain size.

Fig. 13 Dielectric spectra of 8 nm BT ceramic at different frequencies ($T_C = 118\ ℃$).

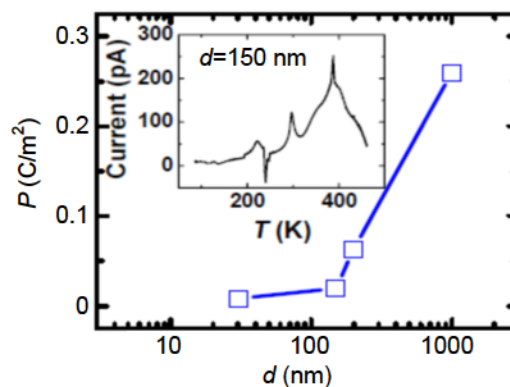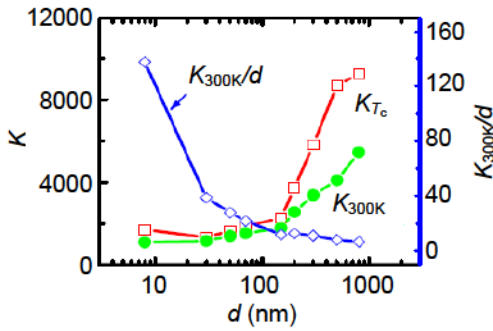**Fig. 14** Grain size effect on switchable polarization of BT ceramics. Inset: depolarization current with peaks at transition temperatures.

At the smallest grain size limit investigated in this study, the 8 nm ceramic does show excellent dielectric properties with three discernible peaks (arrows in Fig. 13) corresponding to the three phase transitions. These peaks are obviously more diffuse than in the GS = 150 nm sample (Fig. 11), but interestingly their frequency dependence is very weak below T_C and nonexistent above T_C. So the diffuseness cannot be attributed to a broad distribution of polarization relaxation time, i.e., it is not a relaxor. The small dielectric loss (typically < 2%) is consistent with the high resistivity (7.8× 10^{11} Ω·cm) and the dense, single-phase microstructure revealed by the TEM micrograph (Fig. 3(a)). On the other hand, despite the robust dielectric properties, the switchable polarization measured by integrating the depolarization current after poling (under 0.1 MV/m during cooling from 500 K to 77 K) is very small in the GS = 8 nm sample (Fig. 14), indicating its ferroelectricity is severely clamped, making temperature-dependent spontaneous depolarization difficult.

The technological driving force toward nanograin

MLCC ceramics comes from not only component miniaturization but also performance. The figure of merit of a capacitor may be defined as the capacitance per unit volume, scaled with K/t^2, where t is the layer thickness of the capacitor. In very thin capacitors, dielectric breakdown is a concern, so the stored charge per unit volume at the breakdown electrical field E_b, KE_b/t, may be taken as an alternative figure of merit. Either measure demands thinner layers, but thinner layers must have a correspondingly smaller ceramic grain size (GS = d) to ensure reliable properties and smooth layer interfaces. Typically $t/d = 6–10$. Therefore, the figure of merit scales with K/d since E_b and t/d are nearly constant. As described above, undoped BT ceramic of GS = 8 nm displays a robust K–temperature performance, with a very low dielectric loss and clear evidence of multiple dielectric/ferroelectric transitions. This nanograin ceramic exhibits a higher figure of merit at 25 ℃ than the state-of-the-art MLCC ceramics featuring GS = 100 nm (Fig. 15). Such reassuring results encourage the continuing march of the MLCC development down the road of nanograin ceramics.
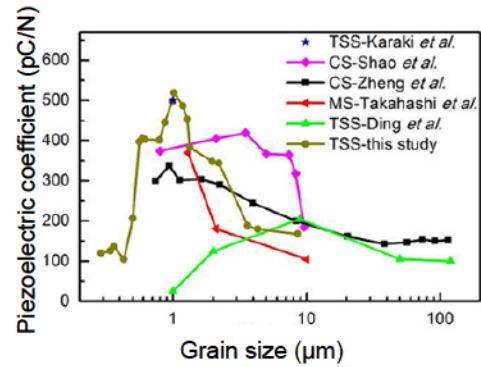
Fig. 15 Relative dielectric constant K and figure of merit (K/d) of BT ceramics of different grain size (GS = d).

3. 2. 2 Piezoelectric properties

BT-based ceramics have been known to show modest piezoelectric activity, with a piezoelectric coefficient (d_{33}) of about 190 pC/N, much less than that of commercial PZT ceramics [78]. Recently, high d_{33} values (338 pC/N, 460 pC/N and 500 pC/N) have been obtained in BT ceramics at GS = 0.94 μm, 1.6 μm and 1 μm, respectively [79−81]. This is believed to be related to the domains in the ceramics. In addition, it is known that d_{33} values decrease from 420 pC/N to 185 pC/N when the average grain size increases from 7 μm to 19 μm, while the average domain width remains approximately constant at around 480 nm [82]. Therefore, the piezoelectric properties of BT can be enhanced by controlling grain size and the corresponding domain structure. Since there is little information about the grain size dependence of piezoelectric properties and domain structures in BT ceramics at grain size below 700 nm, we have undertaken the following study using a similar series of dense BT ceramics as those described above for dielectric properties [57].

Table 5 lists the relative density (ρ_0), average grain size, macroscopic d_{33} and K of various BT ceramics studied. The grain size dependence of d_{33} is shown in Fig. 16, which confirms that d_{33} is enhanced by a decreasing grain size, but the maximum d_{33} (519 pC/N) is reached at around 1 μm below which it rapidly drops with a further decrease in grain size. The d_{33} values from previous studies [79−84] are also plotted in Fig. 16 for comparison; unlike our data they failed to give a clear indication of the d_{33} maximum because their smallest grain size was limited to about 1 μm. Thus, using the TSS technology to obtain finer-grain BT ceramics, we have firmly established the range of optimal grain size for d_{33}: d_{33} = 400−519 pC/N at GS = 500−1000 nm—the value of 519 pC/N being superior to all those reported in prior studies.
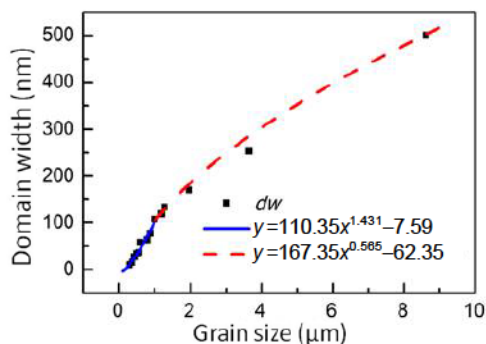

Fig. 16 d_{33} dependence on grain size of BT ceramics (CS, MS and TSS are abbreviations of conventional sintering, microwave sintering and two-step sintering, respectively).

Table 5   Relative density, average grain size, piezoelectric coefficient d_{33} and dielectric constant K for various BaTiO$_3$ ceramics prepared by TSS, using T_1 and T_2 (for t_2) schedules

T_1 (℃)	T_2 (℃)	t_2 (h)	ρ_0 (%)	GS (μm)	K	d_{33} (pC/N)
1250	800	24	95.4	0.29	3660	120
1250	850	24	95.7	0.34	3883	126
1250	900	24	96.4	0.36	4133	137
1250	950	24	96.6	0.43	4207	105
1250	1000	24	96.8	0.50	4794	207
1280	800	24	96.6	0.56	4839	397
1280	850	24	96.9	0.59	5034	407
1280	900	24	96.7	0.62	5126	403
1280	950	24	97.1	0.79	5144	401
1280	1000	24	96.5	0.87	5284	446
1310	800	24	96.4	0.99	6079	498
1310	850	24	96.4	1.02	6487	519
1310	900	24	96.8	1.19	5366	486
1310	950	24	98.9	1.28	5018	453
1310	1000	24	98.6	1.34	4860	383
1340	900	24	98.0	1.97	4072	348
1340	950	24	97.4	2.21	3733	344
1340	1000	24	96.9	3.64	2137	188
1340	1050	24	96.8	4.32	1834	180
1340	1100	24	96.5	8.61	1650	168

It is known that the piezoelectric properties of ceramics may have an extrinsic contribution due to the motion of ferroelectric domain walls [85,86]. Using computer simulation, Ahluwalia et al. [87] investigated a model ferroelectric and showed that the piezoelectric coefficient is enhanced by reducing the domain size. Supporting experimental evidence was observed by Wada et al. [88] in BT single crystals and by Takahashi et al. [89] in microwave-sintered BT ceramics, correlating superior piezoelectric properties to small domain sizes. To investigate the grain size effect on d_{33}, we examined the domain configurations of BT ceramics as a function of grain size using TEM [57]. The domain width (dw) is found to increase with grain size as shown in Fig. 17, and some examples of domain structures are shown in Fig. 18 covering the
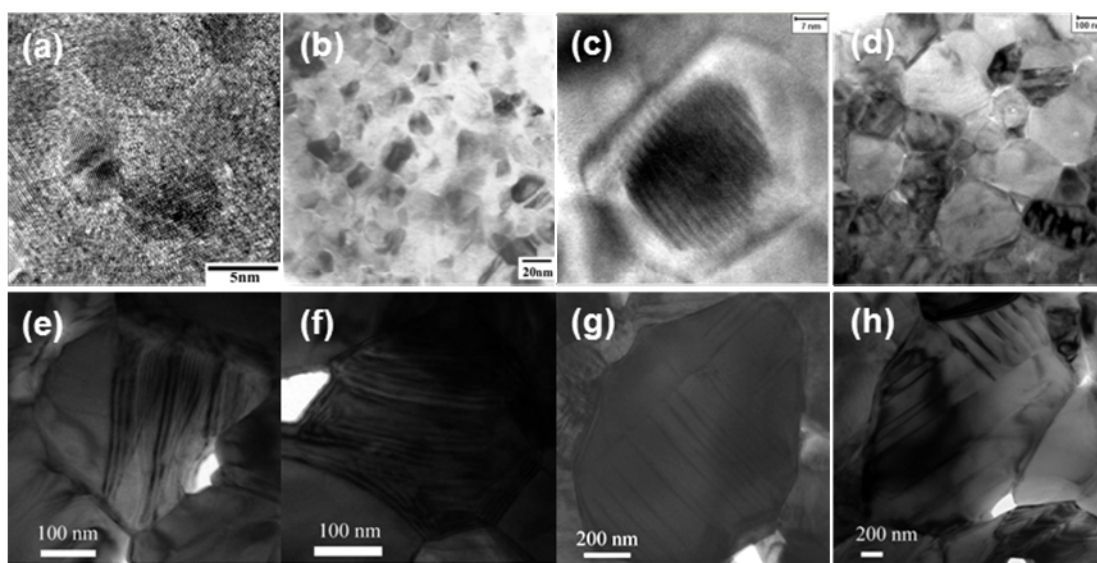
grain size range from 8 nm to 2 μm. Remarkably, nanodomains with size of several to 10 nm are still observed in BT ceramics of the finest grain size, of 8 nm. Moreover, using high-sensitivity piezoresponse force microscopy as a local probe (SPI 4000/ SPA300HV, Seiko, Japan, operated at 2 V AC root-mean-square voltage at 5 kHz, in addition to a DC bias of ±10 V) [16], we observed polarization switching
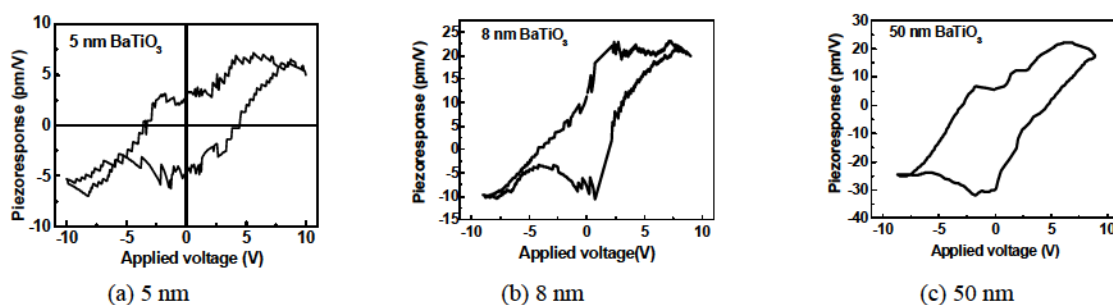

Fig. 17 Domain size dependence of BT ceramics with different grain size. A two-segment curve fit is also shown along with the fitting parameters.

and piezoelectricity in BT nanoceramics at room temperature. Apparently, even with the finest grain size (5 nm), the very high local field near the tip of an atomic force microscope (AFM) can induce ferroelectric hysteresis loops such as those shown in Fig. 19. However, the requisite high field (to overcome the coercive field) when GS < 1 μm proves inaccessible in bulk ceramics making bulk ferroelectricity and piezoelectricity impossible to manifest.

When GS > 1 μm, it is a common observation that the 90° domain width decreases with decreasing grain size. The finer domain width means a larger contribution of domain wall movement to the piezoelectric response, which is favorable for improved piezoelectric properties [90]. On the other hand, when GS < 1 μm, the domain density actually deceases due to the increasing volume fraction of interfaces themselves (domain walls and grain boundaries) and the emergence of monodomains, which coincides with the decrease of d_{33} with decreasing grain size. Moreover, in nanograin ceramics, internal stresses are likely to be another reason that

Fig. 18 TEM micrographs of domain structures of BT ceramics: (a) 8 nm, (b) 20 nm, (c) 50 nm, (d) 100 nm, (e) 290 nm, (f) 360 nm, (g) 990 nm and (h) 1970 nm.

Fig. 19 Typical piezoelectric loops of dense BT ceramics of various grain sizes: (a) 5 nm, (b) 8 nm and (c) 50 nm.

may cause clamping of domains and domain walls. Two-step sintering is nevertheless advantageous since it allows a very precise control of the grain size with excellent size uniformity. This will in turn allow better optimization of piezoelectric response of BT ceramics, which is of considerable interest because BT is lead-free.

4 Microstructures and properties of nano (1−*x*)BiScO₃−*x*PbTiO₃ ceramics

4. 1 Microstructures

As described in Section 2.2, dense BSPT ceramics with an average grain size from 1 μm to 11 nm have been prepared by two-step sintering. Figure 20 shows the X-ray diffraction (XRD) patterns of BSPT ceramics with MPB composition at room temperature. For GS > 60 nm, peak splitting is obvious [31]. Although this is not seen in finer-grain samples because of peak broadening, asymmetry is evident indicating a similar tetragonal distortion still exists in all the samples.
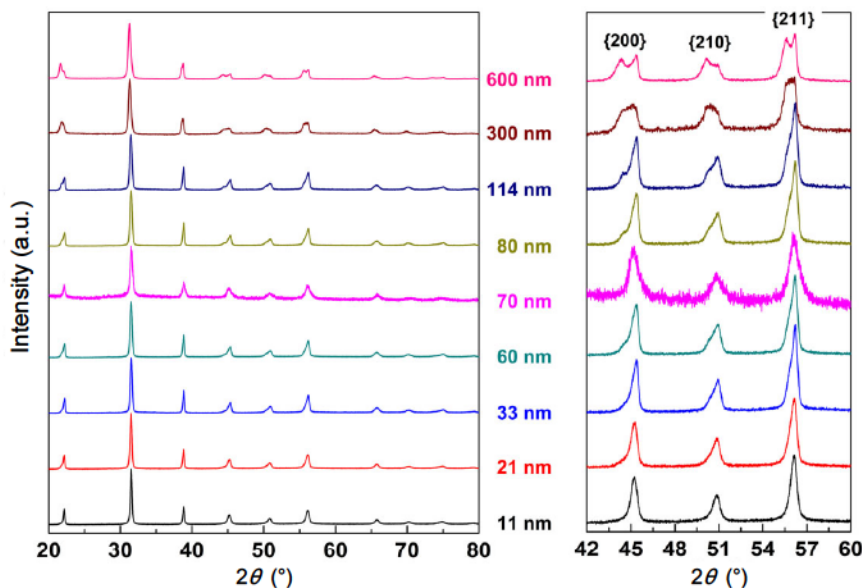
High-resolution synchrotron XRD from 25 ℃ to 500 ℃ was also obtained for BSPT ceramics with grain size from 11 nm to 114 nm. Various structural models were used to fit the data. For example, one can model the XRD of nanograin BSPT by letting it contain a paraelectric cubic phase (perhaps in the grain boundary region) in addition to a tetragonal phase: as

the grain size reduces, the volume fraction of the grain boundary region and hence the cubic phase increase. The refinement results based on different structural models for the 11 nm BSPT sample are listed in Table 6. According to the agreement factors R_{wp} and GOF, the T+M (T for tetragonal and M for monoclinic) phase model was better than the T+R (R for rhombohedral) phase model, and the addition of the cubic (C) phase also improved the refinement, with the c/a ratio of tetragonal distortion slightly increased after the addition [91]. Therefore, the synchrotron data

Table 6 Comparison of refined crystallographic data and agreement factors for BSPT nanoceramics with GS = 11 nm at T = 300 K

Model	Phase fraction (%)	Lattice constant (Å·(°)⁻¹)			R_{wp} (%)	GOF (%)
		T (*P4mm*)	R (*R3m*)/ M (*Cm*)	C (*Pm3m*)		
T+R	55/45	c = 4.0472 a = 4.0154	a = 4.0252 β = 89.94	—	3.61	9.48
T+R+C	33/28/39	c = 4.0645 a = 4.0056	a = 4.0273 β = 89.99	a = 4.02761	2.89	6.11
T+M	53/47	c = 4.0434 a = 4.0168	a = 5.6865 b = 5.6459 c = 4.0777 β = 89.94	—	2.56	4.81
T+M+C	28/42/30	c = 4.0524 a = 4.0121	a = 5.6927 b = 5.6426 c = 4.0803 β = 89.96	a = 4.0281	2.39	4.19
T+M (1.5 μm)	34/66	c = 4.0852 a = 3.9929	a = 5.6592 b = 5.6589 c = 4.0589 β = 89.673	—	7.87	3.38

T: *P4mm*; R: *R3m*; M: *Cm*; C: *Pm3m*. For comparison, the results for a coarse-grain ceramic with GS = 1.5 μm are also listed.

Fig. 20 XRD patterns of BSPT ceramics with different grain sizes.

confirmed the existence of the tetragonal phase, and very likely it coexists with the monoclinic phase. This is similar to the case of Pb(Zr,Ti)O$_3$ (PZT) and Pb(Mg,Nb)O$_3$–PbTiO$_3$ (PMN–PT), two well-known ferroelectric ceramics near their respective morphotropic phase boundaries, which also comprise T and M phases [92]. The structure parameters of the coarse-grain ceramics (GS = 1.5 μm) were also refined and are presented in Table 6, which are consistent with the literature values [93,94]. Comparing these results, it is seen that the tetragonal distortion (c/a-1) of BSPT is significantly reduced in nanograin ceramics.

Figure 21 shows the temperature dependence of the phase fraction of BSPT ceramics with different grain size according to the synchrotron XRD. At GS < 33 nm, the T, M and C phases coexist throughout the range of temperature studied (25–500 ℃). In particular, the ferroelectric T phase persists at 500 ℃, above the Curie temperature 450 ℃, in both 11 nm and 21 nm ceramics. In contrast, when GS = 114 nm, T and M phases disappear at 450 ℃, giving way to the cubic phase at higher temperatures.

4.2 Size effect on ceramic properties

4.2.1 Dielectric properties

Dielectric properties of BSPT ceramics have not been widely reported especially regarding their grain size dependence in the nanoscale. Figure 22 shows the temperature spectra of dielectric constant and loss at 100 kHz of BSPT ceramics with MPB composition at grain size ranging from 11 nm to 1.5 μm. The dielectric anomaly associated with the ferroelectric transition is clearly observed in all the samples, but it is also severely flattened and broadened at smaller grain size despite the fact that the Curie temperature remains almost unchanged, at $T_C \approx 437$ ℃.

4.2.2 Ferroelectric properties

Polarization–electric field (P–E) hysteresis loops of coarse-grain (0.5 μm and 1.5 μm) BSPT ceramics (at the MPB composition) have a classic shape of square loops that are nearly saturated at large fields (Fig. 23(a)). When the grain size reduces to less than 100 nm, however, polarization loops become much narrower and rounded indicating suppression of
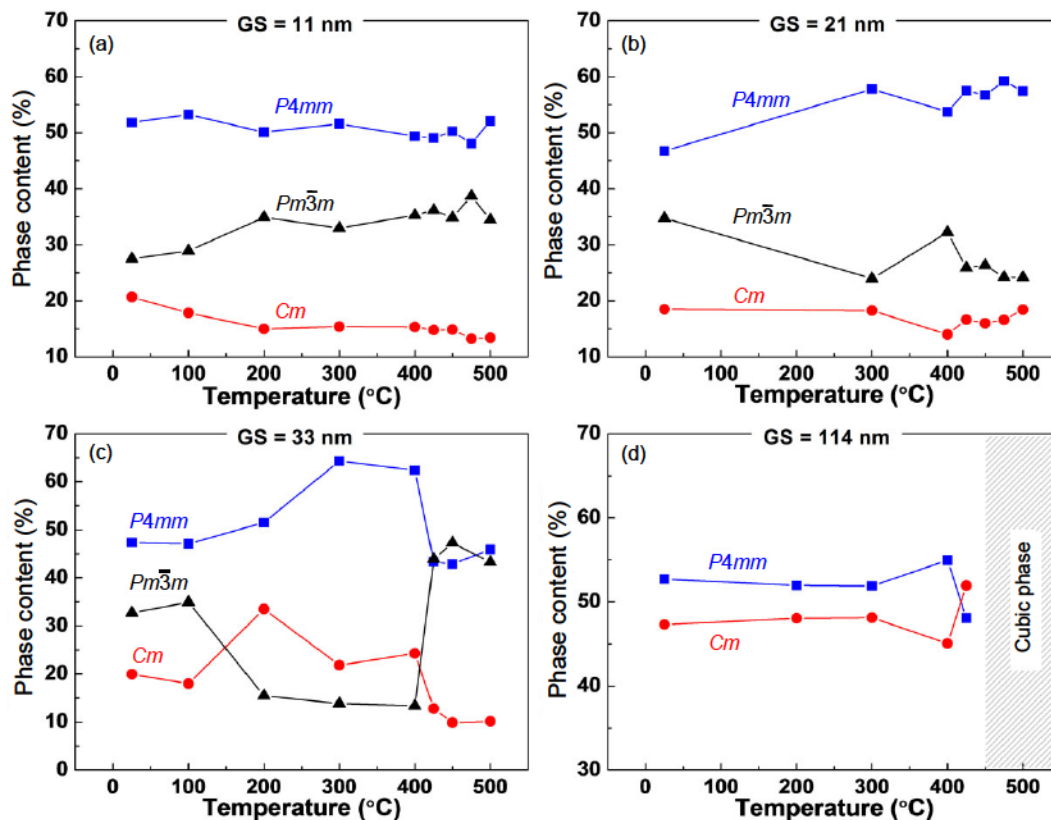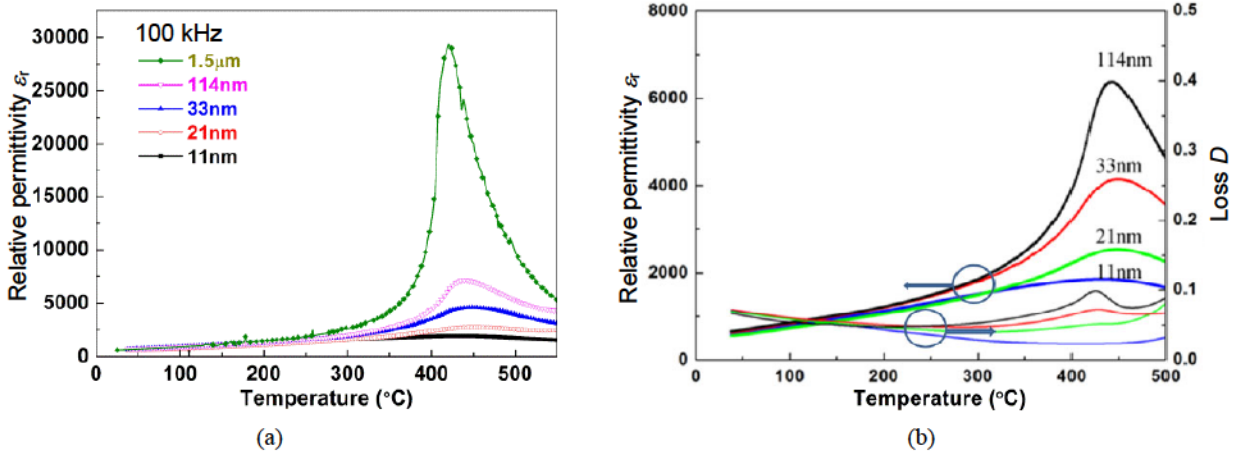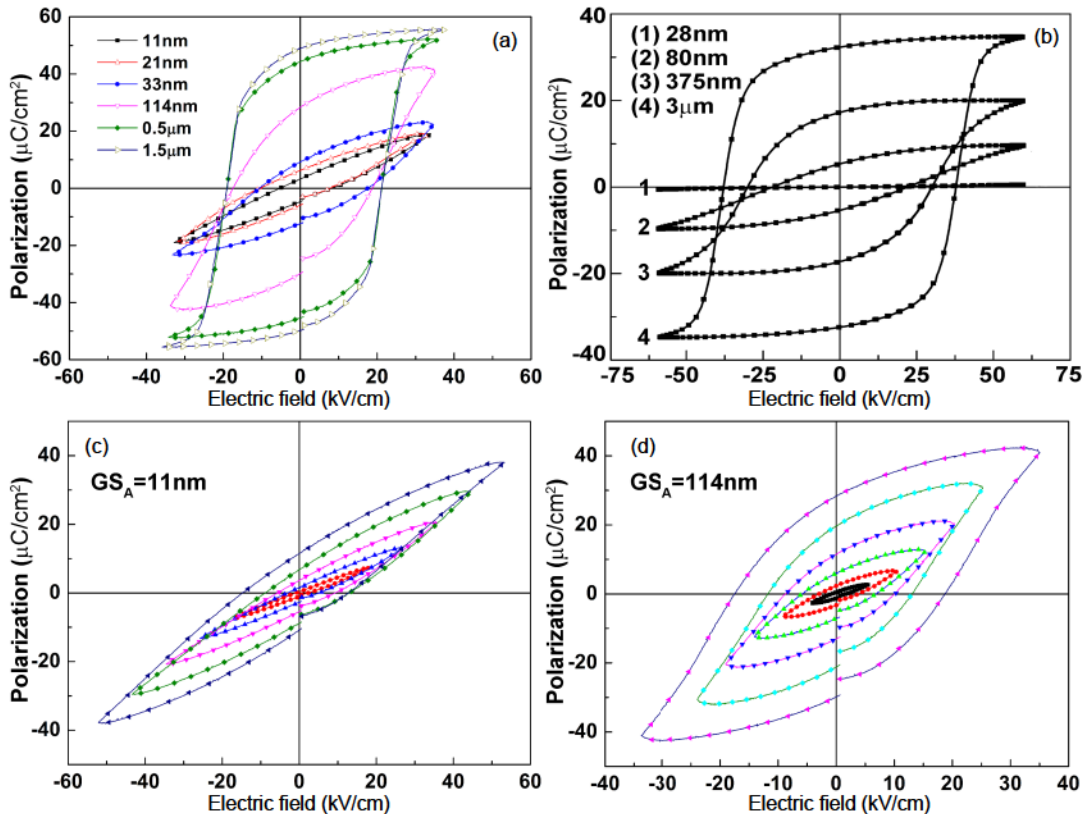

Fig. 21 Phase fraction of BSPT ceramics with different grain sizes.

polarization switching. Similar results were observed in BSPT ceramics of a comparable composition prepared by SPS, reported by Amorín *et al.* [60], as shown in Fig. 23(b). Although polarization saturation is evident in Fig. 23(b) at large fields showing a monotonically decreasing saturation polarization as grain size decreases to 28 nm, no saturation is apparent even at 60 kV/cm in finer-grain ceramics (e.g.,

GS = 11 nm) according to our data (Fig. 23(c)). This sequence of progressive clamping of polarization switching is also apparent in Fig. 23(d) for the same ceramic but at GS = 114 nm, which shows some evidence of polarization saturation albeit at a relatively small polarization. Such clamping may be attributed to the increasing fraction of dielectrically inactive (nonpolar) grain boundaries in nanograin ceramics.

(a)   (b)

Fig. 22   Grain size effect on dielectric properties of BSPT ceramics: (a) temperature spectra of dielectric constant with grain size ranging from nanometer to micrometer; (b) the same as (a) for nanograin ceramics, along with their dielectric loss.

Fig. 23   (a) Grain size effect on the hysteresis loops of BSPT ceramics obtained by two-step sintering method; (b) the same as (a) according to Ref. [60]; (c) and (d) hysteresis loops at increasing fields of BSPT ceramics with GS = 11 nm and 114 nm, respectively.

Since the applied voltage is mostly spent in the nonpolar region, the effective field available for polarization switching in the polar region is greatly reduced; i.e., it may be explained by the "dead layer" effect. (The interpretation in the literature [60] in terms of "exceptionally high resistivity" of the grain boundaries with the smallest grain size, thus resulting in screening of the "electric field within the grains" is obviously incorrect for a set of capacitors.) In addition, the domain walls are likely to be pinned by grain boundaries and defects, thus "frozen" at finer grain size [13]. Therefore, bulk polarization switching is difficult in nanograin ceramics even though local switching under a much higher field is still possible.

4. 2. 3   Piezoelectric properties

The piezoelectric coefficient (d_{33}) of MPB BSPT ceramics obtained by TSS also manifests a peak (700 pC/N) at an intermediate grain size around 1.5 μm as shown in Fig. 24 [25]. This value is much higher than that of coarse-grain BSPT ceramics (450 pC/N) prepared by conventional sintering methods. Importantly, over a relatively wide range of sub-micrometer grain size of 200–1000 nm, d_{33} can maintain a very high value (above 520 pC/N), which seems to suggest that nanosized domains may contribute to enhanced piezoelectricity [87−89]. Piezoresponse force micrographs of these ceramics did reveal a fine domain structure probably composed of 90° domains of 60–70 nm in width [25]. Therefore, their superior piezoelectric properties could be a result of both the MPB composition ($x = 0.635$) and the small domain size. However, when the grain size further reduces to the nano-scale (less than 100 nm), the piezoelectricity once again decreases rapidly just like the dielectric constant, indicating the same physical mechanism that causes clamping of ferroelectricity in

bulk nanograin ceramics is at play here as well. This is the case at least under the electric field strength (40 kV/cm) used in this study.

Local piezoresponse measurements of BSPT ceramics similar to those of BT ceramics were carried out by scanning probe microscopy (SPM) with a conductive Rh coated Si cantilever (bias voltage V from −100 V to 100 V over a small AC excitation of 5 kHz). Typical butterfly-shaped displacement–voltage ($Z−V$) loops from such measurements are shown in Fig. 25 (blue curves). The effective piezoelectric coefficient d_{33}^* can be estimated from the slope of the curve, exhibiting piezoelectric hysteresis (red curves in Fig. 25). Such measurements confirmed that BSPT nanoceramics (GS = 11 nm) is ferroelectric under a high local field [91]. The effective local piezoelectric coefficient d_{33}^* was 292.9±29.8 pm/V, smaller than that of coarse-grain BSPT ceramics but much larger than the macroscopic d_{33} in Fig. 24. The latter difference is due to the very different electric fields in the two experiments: the SPM electric field is very high but confined in a small region of a dimension commensurate with the tip radius of the cantilever tip, wherein substantial switching of nanodomains and a strong piezoelectric response are possible; such high field cannot be reached in bulk ceramics because of dielectric breakdown.

5   Summary and outlook

Highly dense undoped $BaTiO_3$ and $(Bi,Pb)(Sc,Ti)O_3$ ceramics with average grain size from several micrometers down to 5–10 nm have been successfully prepared by the two-step sintering method, some with additional modifications to aid densification. A pronounced and ubiquitous size effect on the
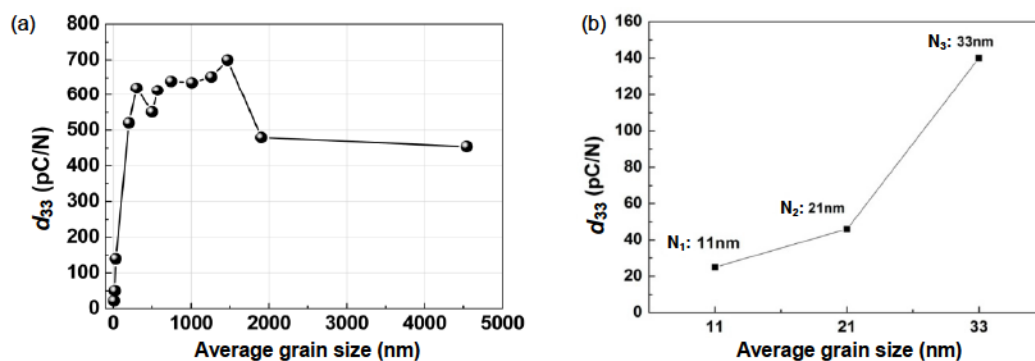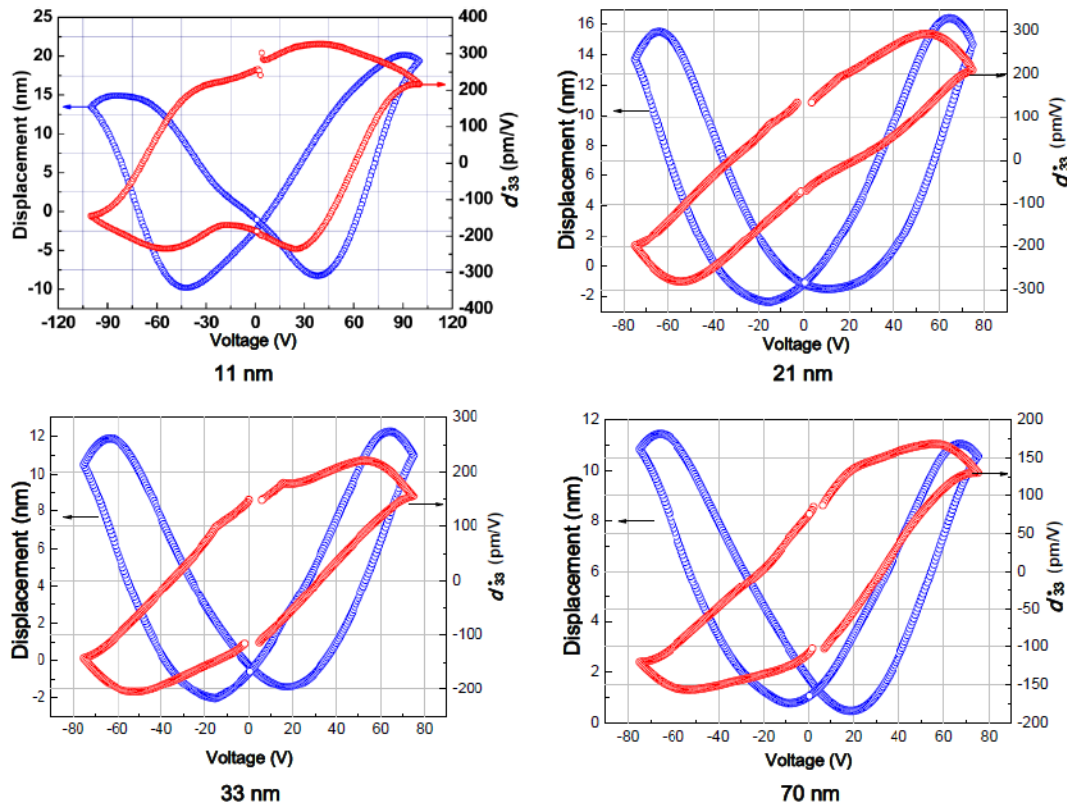

Fig. 24 Grain size effect on macroscopic piezoelectric properties of BSPT ceramics: (a) from micro to nano scale; (b) nano-scale.

Fig. 25   Local piezoelectric response versus applied voltage of BSPT nanoceramics of four grain sizes.

microstructure and ferroelectric properties (including piezoelectric properties and dielectric anomaly) occurring at $GS \approx 1\ \mu m$ and smaller has been established based on the evidence of XRD, HRTEM, AFM, SPM, dielectric constant (K), piezoelectric coefficient (d_{33}) and $P{-}E$ or displacement−voltage hysteresis. Although ferroelectricity and domain switching are substantially suppressed in nanograin ceramics in bulk samples, a strong local field such as that present under the conducting tip of an atomic force microscope or piezoresponse force microscope can induce local domain switching manifesting robust ferroelectricity and piezoelectricity even at a grain size of 5−10 nm. Meanwhile, a flattened but somewhat extended dielectric and piezoelectric anomaly maintaining high responsivity values (K, d_{33}) relatively close to their peak values is also seen at sub-1000 nm grain size. Importantly, this enables nanograin ceramics to exhibit a higher figure of merit at 25 ℃ than the state-of-the-art MLCC ceramics featuring $GS = 100$ nm. Moreover, the confirmation of ferroelectricity at $GS = 5{-}10$ nm avails the possibility of unlocking versatile ferroelectricity-enabled properties provided ingenious means to relieve grain-size-related internal stresses/fields can be constructed. In this way, the fundamental studies reviewed here, made possible by nanograin ceramics obtained by two-step sintering, have provided the essential insight and a most valuable outlook to guide current and future MLCC technology as well as the further development of advanced ferroelectric and piezoelectric devices.

Acknowledgements

ShaoPeng Zhang and Hui Zhang for their contributions for this work.

References

[1] Cross LE. Dielectric, piezoelectric and ferroelectric components. *Am Ceram Soc Bull* 1984, **63**: 586–590.

[2] Hennings D, Klee M, Waser R. Advanced dielectrics: Bulk ceramics and thin films. *Adv Mater* 1991, **3**: 334–340.

[3] Suzuki K, Kageyama K, Takagi H, *et al.* Fabrication of monodispersed barium titanate nanoparticles with narrow size distribution. *J Am Ceram Soc* 2008, **91**: 1721–1724.

[4] Yoon S, Baik S. Formation mechanisms of tetragonal barium titanate nanoparticles in alkoxide–hydroxide sol-precipitation synthesis. *J Am Ceram Soc* 2006, **89**: 1816–1821.

[5] Kishi H, Mizuno Y, Chazono H. Base-metal electrode-multilayer ceramic capacitors: Past, present and future perspectives. *Jpn J Appl Phys* 2003, **42**: 1–15.

[6] Sakabe Y, Reynolds T. Base-metal electrode capacitors. *Am Ceram Soc Bull* 2002, **81**: 24–26.

[7] Tian ZB, Wang XH, Lee S, *et al.* Microstructure evolution and dielectric properties of ultrafine grained BaTiO₃-based ceramics by two-step sintering. *J Am Ceram Soc* 2011, **94**: 1119–1124.

[8] Uchino K, Sadanaga E, Hirose T. Dependence of the crystal structure on particle size in barium titanate. *J Am Ceram Soc* 1989, **72**: 1555–1558.

[9] Frey MH, Payne DA. Grain size effect on structure and phase transformations for barium titanate. *Phys Rev B* 1996, **54**: 3158–3168.

[10] Saad MM, Baxter P, Bowman RM, *et al.* Intrinsic dielectric response in ferroelectric nano-capacitors. *J Phys: Condens Matter* 2004, **16**: L451–L456.

[11] Ishidate T, Abe S, Takahashi H, *et al.* Phase diagram of BaTiO₃. *Phys Rev Lett* 1997, **78**: 2397–2400.

[12] Zhao Z, Buscaglia V, Viviani M, *et al.* Grain-size effects on the ferroelectric behavior of dense nanocrystalline BaTiO₃ ceramics. *Phys Rev B* 2004, **70**: 024107.

[13] Buscaglia V, Buscaglia MT, Viviani M, *et al.* Raman and AFM piezoresponse study of dense BaTiO₃ nanocrystalline ceramics. *J Eur Ceram Soc* 2005, **25**: 3059–3062.

[14] Polotai AV, Ragulya AV, Randall CA. The XRD and IR study of the barium titanate nano-powder obtained via oxalate route. *Ferroelectrics* 2004, **298**: 243–251.

[15] Buscaglia MT, Viviani M, Buscaglia V, *et al.* High dielectric constant and frozen macroscopic polarization in dense nanocrystalline BaTiO₃ ceramics. *Phys Rev B* 2006, **73**: 064114.

[16] Wang XH, Deng XY, Wen H, *et al.* Phase transition and

[17] Sun TY, Wang XH, Wang H, *et al.* A phenomenological model on phase transitions in nanocrystalline barium titanate ceramic. *J Am Ceram Soc* 2010, **93**: 2571–2573.

[18] Zhang H, Wang XH, Tian ZB, *et al.* Fabrication of monodispersed 5-nm BaTiO₃ nanocrystals with narrow size distribution via one-step solvothermal route. *J Am Ceram Soc* 2011, **94**: 3220–3222.

[19] Eitel RE, Randall CA, Shrout TR, *et al.* New high temperature morphotropic phase boundary piezoelectrics based on Bi(Me)O₃–PbTiO₃ ceramics. *Jpn J Appl Phys* 2001, **40**: 5999–6002.

[20] Goldschmidt V. Skrifter Norske Videnskaps-Akademi. *Oslo, Matemot-Natureid Klasse* 1926, **1**: 7.

[21] Tutuncu G, Damjanovic D, Chen J, *et al.* Deaging and asymmetric energy landscapes in electrically biased ferroelectrics. *Phys Rev Lett* 2012, **108**: 177601.

[22] Gotmare SW, Leontsev SO, Eitel RE. Thermal degradation and aging of high-temperature piezoelectric ceramics. *J Am Ceram Soc* 2010, **93**: 1965–1969.

[23] Sehirlioglu A, Sayir A, Dynys F. High temperature properties of BiScO₃–PbTiO₃ piezoelectric ceramics. *J Appl Phys* 2009, **106**: 014102.

[24] Zou TT, Wang XH, Zhao W, *et al.* Preparation and properties of fine-grain (1−x)BiScO₃−xPbTiO₃ ceramics by two-step sintering. *J Am Ceram Soc* 2008, **91**: 121–126.

[25] Zou TT, Wang XH, Wang H, *et al.* Bulk dense fine-grain (1−x)BiScO₃−xPbTiO₃ ceramics with high piezoelectric coefficient. *Appl Phys Lett* 2008, **93**: 192913.

[26] Grinberg I, Rappe AM. Nonmonotonic T_C trends in Bi-based ferroelectric perovskite solid solutions. *Phys Rev Lett* 2007, **98**: 037603.

[27] Chaigneau J, Kiat JM, Malibert C, *et al.* Morphotropic phase boundaries in (BiScO₃)(1−x)(PbTiO₃)x (0.60 < x < 0.75) and their relation to chemical composition and polar order. *Phys Rev B* 2007, **76**: 094111.

[28] Chen S, Dong XL, Mao CL, *et al.* Thermal stability of (1−x)BiScO₃−xPbTiO₃ piezoelectric ceramics for high-temperature sensor applications. *J Am Ceram Soc* 2006, **89**: 3270–3272.

[29] Inaguma Y, Miyaguchi A, Yoshida M, *et al.* High-pressure synthesis and ferroelectric properties in perovskite-type BiScO₃–PbTiO₃ solid solution. *J Appl Phys* 2004, **95**: 231–235.

[30] Randall CA, Eitel RE, Shrout TR, *et al.* Transmission electron microscopy investigation of the high temperature BiScO₃–PbTiO₃ piezoelectric ceramic system. *J Appl Phys* 2003, **93**: 9271–9274.

[31] Eitel RE, Randall CA, Shrout TR, *et al.* Preparation and characterization of high temperature perovskite ferroelectrics in the solid-solution (1−x)BiScO₃−xPbTiO₃. *Jpn J Appl Phys* 2002, **41**: 2099–2104.

[32] Zhang SJ, Randall CA, Shrout TR. Dielectric and piezoelectric properties of BiScO₃–PbTiO₃ crystals with morphotropic phase boundary composition. *Jpn J Appl Phys* 2004, **43**: 6199–6203.

[33] Zhang SJ, Randall CA, Shrout TR. Dielectric, piezoelectric

and elastic properties of tetragonal BiScO₃–PbTiO₃ single crystal with single domain. *Solid State Commun* 2004, **131**: 41–45.

[34] Zhang SJ, Randall CA, Shrout TR. Electromechanical properties in rhombohedral BiScO₃–PbTiO₃ single crystals as a function of temperature. *Jpn J Appl Phys* 2003, **42**: L1152–L1154.

[35] Zhang SJ, Randall CA, Shrout TR. High Curie temperature piezocrystals in the BiScO₃–PbTiO₃ perovskite system. *Appl Phys Lett* 2003, **83**: 3150–3152.

[36] Zhang SJ, Lebrun L, Rhee S, *et al.* Crystal growth and characterization of new high Curie temperature (1−*x*)BiScO₃−*x*PbTiO₃ single crystals. *J Cryst Growth* 2002, **236**: 210–216.

[37] Zhong CF, Wang XH, Fang JA, *et al.* Investigation of thickness dependence of structure and electric properties of sol–gel-derived BiScO₃–PbTiO₃ thin films. *J Am Ceram Soc* 2010, **93**: 3305–3311.

[38] Zhong CF, Wang XH, Wen H, *et al.* Fabrication and properties of epitaxial growth BiScO₃–PbTiO₃ thin film via a hydrothermal method. *Appl Phys Lett* 2008, **92**: 222910.

[39] Wen H, Wang XH, Zhong CF, *et al.* Epitaxial growth of sol–gel derived BiScO₃–PbTiO₃ thin film on Nb-doped SrTiO₃ single crystal substrate. *Appl Phys Lett* 2007, **90**: 202902.

[40] Wen H, Wang XH, Zhong CF, *et al.* Properties of compositionally graded BiScO₃–PbTiO₃ thin films fabricated by a sol–gel process. *J Am Ceram Soc* 2007, **90**: 2441–2445.

[41] Wen H, Wang XH, Li LT. Orientation control in sol–gel-derived BiScO₃–PbTiO₃ thin films. *J Am Ceram Soc* 2007, **90**: 3248–3254.

[42] Wen H, Wang XH, Deng XY, *et al.* Effect of crystallization process on the ferroelectric properties of sol–gel derived BiScO₃–PbTiO₃ thin films. *J Appl Phys* 2007, **101**: 016103.

[43] Yoshimura T, Trolier-McKinstry S. Growth and properties of (001) BiScO₃–PbTiO₃ epitaxial films. *Appl Phys Lett* 2002, **81**: 2065–2066.

[44] Scott JF. Applications of modern ferroelectrics. *Science* 2007, **315**: 954–959.

[45] Mao YB, Banerjee S, Wong SS. Hydrothermal synthesis of perovskite nanotubes. *Chem Commun* 2003, **3**: 408–409.

[46] Boulosa M, Guillemet-Fritsch S, Mathieu F, *et al.* Hydrothermal synthesis of nanosized BaTiO₃ powders and dielectric properties of corresponding ceramics. *Solid State Ionics* 2005, **176**: 1301–1309.

[47] Chen IW, Wang XH. Sintering dense nanocrystalline ceramics without final-stage grain growth. *Nature* 2000, **404**: 168–171.

[48] Wang DL, Zhu KJ, Ji HL, *et al.* Two-step sintering of the pure K₀.₅Na₀.₅NbO₃ lead-free piezoceramics and its piezoelectric properties. *Ferroelectrics* 2009, **392**: 120–126.

[49] Mazaheri M, Zahedi AM, Haghighatzadeh M, *et al.* Sintering of titania nanoceramic: Densification and grain growth. *Ceram Int* 2009, **35**: 685–691.

[50] Maca K, Pouchly V, Zalud P. Two-step sintering of oxide ceramics with various crystal structures. *J Eur Ceram Soc* 2010, **30**: 583–589.

[51] Wang XH, Deng XY, Bai HL, *et al.* Two-step sintering of ceramics with constant grain-size, II: BaTiO₃ and Ni–Cu–Zn ferrite. *J Am Ceram Soc* 2006, **89**: 438–443.

[52] Wang XH, Chen IW. Sintering of nanoceramics. In *Nanomaterials Handbook.* Gogotsi Y, Ed. New York: Taylor Francis, 2006: 359–382.

[53] Kim HD, Han BD, Park DS, *et al.* Novel two-step sintering process to obtain a bimodal microstructure in silicon nitride. *J Am Ceram Soc* 2002, **85**: 245–252.

[54] Wang XH, Chen PL, Chen IW. Two-step sintering of ceramics with constant grain-size, I. Y₂O₃ . *J Am Ceram Soc* 2006, **89**: 431–437.

[55] Wang XH, Deng XY, Zhou H, *et al.* Bulk dense nanocrystalline BaTiO₃ ceramics prepared by novel pressureless two-step sintering method. *J Electroceram* 2008, **21**: 230–233.

[56] Li LT, Wang XH, Zhang H, *et al.* Size effect investigation on nano-scale ferroelectric ceramic materials. Proceeding of 8th International Conference and Tabletop Exhibition on Ceramic Interconnect and Ceramic Microsystems Technologies (CICMT 2012) Erfurt, Germany, April 16–19, 2012: 000216–000221.

[57] Huan Y, Wang XH, Fang J, *et al.* Grain size effects on piezoelectric properties and domain structure of BaTiO₃ ceramics prepared by two-step sintering. *J Am Ceram Soc* 2013, **96**: 3369–3371.

[58] Huan Y, Wang XH, Fang J, *et al.* Grain size effect on piezoelectric and ferroelectric properties of BaTiO₃ ceramics. *J Eur Ceram Soc* 2014, **34**: 1445–1448.

[59] Algueró M, Amorín H, Hungría T, *et al.* Macroscopic ferroelectricity and piezoelectricity in nanostructured BiScO₃–PbTiO₃ ceramics. *Appl Phys Lett* 2009, **94**: 012902.

[60] Amorín H, Jiménez R, Ricote J, *et al.* Apparent vanishing of ferroelectricity in nanostructured BiScO₃–PbTiO₃. *J Phys D: Appl Phys* 2010, **43**: 285401.

[61] Zhang SP, Wang XH, Wang H, *et al.* Grain boundary region and local piezoelectric response of BiScO₃–PbTiO₃ nanoceramics prepared by combination of SPS and two-step sintering. *J Eur Ceram Soc* 2014, **34**: 2317–2323

[62] Wang XH, Zhang SP, Li LT. Piezoelectric nanoceramics. In *Springer Handbook of Nanomaterials.* Vajtai R, Ed. Berlin Heidelberg: Springer, 2013: 553–570.

[63] Burns G, Scott BA. Raman studies of underdamped soft modes in PbTiO₃. *Phys Rev Lett* 1970, **25**: 167–169.

[64] Fu D, Suzuki H, Ishikawa K. Size-induced phase transition in PbTiO₃ nanocrystals: Raman scattering study. *Phys Rev B* 2000, **62**: 3125–3129.

[65] Pirc R, Blinc R. Off-center Ti model of barium titanate. *Phys Rev B* 2004, 70: 134107 .

[66] Keramidas VG, White WB. Raman scattering from Ca$_x$Zr$_{1-x}$O$_{2-x}$□$_x$, a system with massive point defects. *J Phys Chem Solids* 1973, **34**: 1873–1878.

[67] Li P, Chen I-W, Penner-Hahn JE. X-ray absorption studies of zirconia polymorphs I. Characteristic local structures. *Phys Rev B* 1993, **48**: 10063–10073.

[68] Li P, Chen I-W, Penner-Hahn JE.   X-ray absorption studies of zirconia polymorphs II. Effects of Y_2O_3 dopant on ZrO_2 structure. *Phys Rev B* 1993, **48**: 10074–10081.

[69] Li P, Chen I-W, Penner-Hahn JE. The effects of dopants on zirconia stabilization—An X-ray absorption study I. Trivalent dopants. *J Am Ceram Soc* 1994, **77**: 118–128.

[70] Shirane G, Frazer BC, Minkiewicz VJ, *et al.* Soft optic modes in barium titanate. *Phys Rev Lett* 1967, **19**: 234–238.

[71] DiDomenico M, Wemble SH, Porto SPS. Raman spectrum of single-domain $BaTiO_3$. *Phys Rev* 1968, **174**: 522–523.

[72] Zhu JL, Han W, Wang XH, *et al.* Phase coexistence evolution of nano $BaTiO_3$ as function of particle sizes and temperatures. *J Appl Phys* 2012, **112**: 064110.

[73] Larson AC, von Dreele RB. General structure analysis system (GSAS). Los Alamos National Laboratory Report LAUR, 2004: 86–748.

[74] Kwei GH, Lawson AC, Billinge SJL, *et al.* Structures of the ferroelectric phases of barium–titanate. *J Phys Chem* 1993, **97**: 2368–2377 .

[75] Lin S, Lu TQ, Jin CQ, *et al.* Size effect on the dielectric properties of $BaTiO_3$ nanoceramics in a modified Ginsburg–Landau–Devonshire thermodynamic theory. *Phys Rev B* 2006, **74**: 134115.

[76] Buscaglia MT, Buscaglia V, Viviani M, *et al.* Ferroelectric properties of dense nanocrystalline $BaTiO_3$ ceramics. *Nanotechnology* 2004, **15**: 1113.

[77] Kinoshita K, Yamaji A. Grain-size effects on dielectric properties in barium–titanate ceramics. *J Appl Phys* 1976, **47**: 371–373.

[78] Jaffe B, Cook WR, Jaffe H. Piezoelectric ceramics. London: Academic Press, 1971.

[79] Zheng P, Zhang JL, Tan YQ, *et al.* Grain-size effects on dielectric and piezoelectric properties of poled $BaTiO_3$ ceramics. *Acta Mater* 2012, **60**: 5022–5030 .

[80] Karaki T, Yan K, Adachi M. Barium titanate piezoelectric ceramics manufactured by two-step sintering. *Jpn J Appl Phys* 2007, **46**: 7035–7038.

[81] Karaki T, Yan K, Adachi M. Subgrain microstructure in high-performance $BaTiO_3$ piezoelectric ceramics. *Appl Phys Express* 2008, **1**: 111402.

[82] Shao SF, Zhang JL, Zheng Z, *et al.* High piezoelectric properties and domain configuration in $BaTiO_3$ ceramics obtained through the solid-state reaction route. *J Phys D: Appl Phys* 2008, **41**: 125408.

[83] Takahashi H, Numamoto Y, Tani J, *et al.* Considerations for $BaTiO_3$ ceramics with high piezoelectric properties fabricated by microwave sintering method. *Jpn J Appl Phys* 2008, **47**: 8468–8471.

[84] Ding SH, Song TX, Yang XJ, *et al.* Effect of grain size of $BaTiO_3$ ceramics on dielectric properties. *Ferroelectrics* 2010, **402**: 55–59.

[85] Arlt G, Hennings D, de With G. Dielectric properties of fine-grained barium titanate ceramics. *J Appl Phys* 1985, **58**: 1619–1625.

[86] Randall CA, Kim N, Kucera JP, *et al.* Intrinsic and extrinsic size effects in fine-grained morphotropic-phase-boundary lead zirconate titanate ceramics. *J Am Ceram Soc* 1998, **81**: 677–688.

[87] Ahluwalia R, Lookman T, Saxena A, *et al.* Domain-size dependence of piezoelectric properties of ferroelectrics. *Phys Rev B* 2005, **72**: 014112.

[88] Wada S, Yako K, Kakemoto H, *et al.* Enhanced piezoelectric properties of barium titanate single crystals with different engineered-domain sizes. *J Appl Phys* 2005, **98**: 014109.

[89] Takahashi H, Numamoto Y, Tani J, *et al.* Lead-free barium titanate ceramics with large piezoelectric constant fabricated by microwave sintering. *Jpn J Appl Phys* 2006, **45**: 7405.

[90] Sato Y, Hirayama T, Ikuhara Y. Evolution of nanodomains under DC electrical bias in $Pb(Mg_{1/3}N_{b2/3})O_3$–$PbTiO_3$: An *in-situ* transmission electron microscopy study. *Appl Phys Lett* 2012, **100**: 172902.

[91] Zhang SP, Wang XH, Zhu JL, *et al.* The microstructure and ferroelectricity of $BiScO_3$–$PbTiO_3$ nanoceramics at morphotropic phase boundaries. *Scripta Mater* 2014, **82**: 45–48.

[92] Noheda B, Cox D, Shirane G, *et al.* Stability of the monoclinic phase in the ferroelectric perovskite $PbZr_{1-x}Ti_xO_3$. *Phys Rev B* 2000, **63**: 14103.

[93] Shahzad K, Li LH, Li ZR, *et al.* Structural characterization and dielectric properties of sol–gel synthesized $BiScO_3$–$0.64PbTiO_3$ ceramics. *Ferroelectrics* 2010, **402**: 142–149.

[94] Datta K, Walker D, Thomas PA. Structural investigations of the bismuth scandate–lead titanate $xBiScO_3$–$(1-x)PbTiO_3$ solid solution for $0.10 \leqslant x \leqslant 0.40$. *Phys Rev B* 2010, **82**: 144108.